J|A|C|S
ARTICLES
Published on Web 01/04/2002

Architectural Control of Magnetic Semiconductor Nanocrystals

Young-wook Jun, Yoon-young Jung, and Jinwoo Cheon*

Contribution from the Department of Chemistry and School of Molecular Science (BK21), Korea Advanced Institute of Science and Technology, Taejon 305-701, Korea

Received August 20, 2001

Abstract: Shape- and dopant-controlled magnetic semiconductor nanocrystals have been achieved by the thermolysis of nonpyrophoric and less reactive single molecular precursors under a monosurfactant system. Reaction parameters governing both the intrinsic crystalline phase and the growth regime (kinetic vs thermodynamic) are found to be important for the synthesis of various shapes of MnS nanocrystals that include cubes, spheres, 1-dimensional (1-D) monowires, and branched wires (bipods, tripods, and tetrapods). Obtained nanowires exhibit enhanced optical and magnetic properties compared to those of 0-D nanospheres. Proper choice of molecular precursors and kinetically driven low-temperature growth afford dopant controlled 1-D $Cd_{1-x}Mn_xS$ nanorods at high levels (up to ~12%) of Mn, which is supported by repeated surface exchange experiments and X-ray diffraction (XRD) and electron paramagnetic resonance (EPR) analyses.

Introduction

In the nanoscale regime, the size and shape of materials strongly influence their physical properties.[1] In particular, one-dimensional (1-D) semiconductor nanocrystals not only exhibit novel optical and magnetic properties but also are key components in the fabrication of nanodevices. For example, 1-D CdSe exhibit linearly polarized emission, while 1-D magnetic nanocrystals have higher blocking temperatures and larger magnetization coercivities when compared with their 0-D counterparts.[2] One-dimensional wires of InP have been utilized as key materials in addressable two-terminal circuits for LED applications.[3] On the other hand, the use of both the spin and the charge of electrons in semiconductors has long been sought after as ideal components for the storage and processing of information for electronic devices. One of the candidates is the diluted magnetic semiconductors (DMS). Transition metal-doped DMSs show novel optomagnetic phenomena, and also the spin state and the transport of the carriers can potentially be tailored for spintronic applications.[4]

Architectural control of the anisotropic nanocrystals including 1-D wires and the reliable incorporation of desired dopants are imperative for the success of bottom-up nanodevice applications, not to mention the novel scientific features that accompany them. Therefore, the development of not only facile but also controllable synthetic methods in these matters is of significance.

In this paper, we demonstrate a unique synthetic method that yields shape-controlled MnS nanocrystals as well as 1-D DMS, $Cd_{1-x}Mn_xS$ nanorods. We first study a transition metal-based MnS magnetic semiconductor system in order to gain a better understanding of the shape-guiding growth mechanisms. The architecture of our MnS nanocrystals can be varied between spheres (0-D), monowires (1-D), branched wires (bipods, tripods, tetrapods), and cubes (0-D). The MnS nanocrystals are subsequently used as an efficient dopant in the DMS CdS nanorod formation in which homogeneous distributions of Mn dopant are successfully achieved. We utilize nonpyrophoric and less reactive alternative molecular precursors that enable the kinetic control of crystal growth through a low-temperature pyrolytic process.

Experimental Section

General Methods. All procedures were carried out by standard airless techniques under argon. $Cd(S_2CNEt_2)_2$ and $Mn(S_2CNEt_2)_2$ were prepared according to literature methods.[5] All reagents and solvents were purified by standard techniques. Hexadecylamine (HDA) was dried and degassed by heating at 120 °C before use.

Synthesis of MnS Nanocrystals: (A) Branched Nanowires. A warm solution (~70 °C) of 0.3 g of HDA including 30 mg of $Mn(S_2CNEt_2)_2$ is injected into a hot solution (120 °C) of ~0.5 g of HDA. After mixing, the colorless solution rapidly changes to pink. After 20

* Corresponding author: e-mail jcheon@kaist.ac.kr.

(1) (a) Brus, L. E. *J. Chem. Phys.* **1984**, *80*, 4403. (b) Murray, C. B.; Norris, D. J.; Bawendi, M. G. *J. Am. Chem. Soc.* **1993**, *115*, 8706. (c) Alivisatos, A. P. *J. Phys. Chem.* **1996**, *100*, 13226. (d) Markovich, G.; Collier, C. P.; Henrichs, S. E.; Remacle, F.; Levine, R. D.; Heath, J. R. *Acc. Chem. Res.* **1999**, *32*, 415.

(2) (a) Peng, X.; Manna, L.; Wang, W.; Wichham, J.; Scher, E.; Kadavanich, A.; Alivisatos, A. P. *Nature* **2000**, *404*, 59. (b) Peng, Z. A.; Peng, X. *J. Am. Chem. Soc.* **2001**, *123*, 1389. (c) Hu, J.; Li, L.-S.; Yang, W.; Manna, L.; Wang, L.-W.; Alivisatos, A. P. *Science* **2001**, *292*, 2060. (d) Park, S. J.; Kim, S.; Lee, S.; Khim, Z. G.; Char, K.; Hyeon, T. *J. Am. Chem. Soc.* **2000**, *122*, 8581. (e) Puntes, V. F.; Krishnan, K. M.; Alivisatos, A. P. *Science* **2001**, *291*, 2115. (f) Manna, L.; Scher, E. C.; Alivisatos, A. P. *J. Am. Chem. Soc.* **2000**, *122*, 12700.

(3) Duan, X.; Huang, Y.; Cui, Y.; Wang, J.; Lieber, C. M. *Nature* **2001**, *409*, 66.

(4) (a) Ohno, H. *Science* **1998**, *281*, 951. (b) Samarth, N.; Furdyna, J. K. *Phys. Rev. B* **1988**, *37*, 9227. (c) Dietl, T.; Ohno, H.; Matsukura, F.; Clibert, J.; Ferrand, D. *Science* **2000**, *287*, 1019. (d) Awschalom, D. D.; Kawakami, R. K. *Nature* **2000**, *408*, 923.

(5) Ciampolini, M.; Mengozzi, C.; Orioli, O. *J. Chem. Soc., Dalton Trans.* **1975**, 2051.

min, the reaction solution is cooled to 70 °C and treated with ethanol to generate pink flocculates that are separated by centrifugation. Nanocrystals are obtained as pink powders and redispersed in dichloromethane. Without further size sorting, obtained nanowires are moderately monodispersed with unique forms.

(B) Nanospheres and Nanocubes. Nanospheres and nanocubes are obtained by the same procedures used to prepare nanowires except for the different growth temperatures of ~180 and 250 °C, respectively. Nanospheres can also be prepared by prolonged reaction of ~2 h at ~150 °C.

Synthesis of $Cd_{1-x}Mn_xS$ Nanocrystals. $Cd(S_2CNEt_2)_2$ (0.200 g, 0.570 mmol) dissolved in 0.3 mL of octylamine and an aliquot amount of dopant precursor solution (0.294 M of $Mn(S_2CNEt_2)_2$ in octylamine) are first mixed, where the amount of dopant solution is varied between 0.04, 0.1, 0.2, and 0.3 mL in order to control the Mn concentration in the final $Cd_{1-x}Mn_xS$. Then the combined solution containing both the precursors in appropriate ratio was rapidly injected into a hot solution (~120 °C) of 0.5 g of HDA. After 10 min, the orange-yellow reaction mixture was treated with ethanol to generate nanocrystals that were isolated by centrifugation. Obtained nanocrystals are readily redispersed in toluene. Surface exchange experiments with pyridine are performed according to literature methods.[6]

Characterization. Transmission electron microscopy (TEM) observations and energy dispersive analyses of X-ray emission (EDAX) were carried out on an EM 912 Omega (KBSI) and Hitachi H9000-NAR high-resolution electron microscope operated at 80 or 300 kV, respectively. UV−Vis absorption data were obtained by a Shimadzu UV-3100S spectrophotometer in toluene, and photoluminescence spectra were collected by a Perkin-Elmer LS50 luminescence spectrometer. Low-temperature (77 K) electron paramagnetic resonance (EPR) spectra were obtained by a Bruker ESP 300S instrument. Powder X-ray diffraction (XRD) patterns were obtained with graphite-monochromatized Cu Kα radiation in a Rigaku Miniflex diffractometer operated at 40 kV and 80 mA. Magnetic measurements were performed on a SQUID magnetometer (Quantum Design MPMS-7). DC susceptibility and hysteresis measurements were recorded for powdered samples of nanoparticles in a gelatin capsule. The temperature was varied between 5 and 300 K according to a zero-field cooling (ZFC) procedure at 75 Oe, and the hysteretic loops were obtained in a magnetic field varying from +5 to −5 T.

Results and Discussion

Various shapes of MnS 1-D based nanocrystals are grown from the thermal decomposition of a single molecular precursor, $Mn(S_2CNEt_2)_2$, in a hexadecylamine (HDA) monosurfactant system. At low growth temperatures (~120 °C) and reaction times (~20 min), wires of 2.2 ± 0.2 nm in width with aspect ratios of ~80 are obtained (Figure 1A). Along with the monowires, other shapes including bipods (~25%, Figure 1B), tripods (~20%, Figure 1C), and tetrapods (6%, Figure 1D) are observed. The formation of a network pattern seems to be governed by the branched wires (bipods and tripods) that constitute the skeletons of the assembly upon which monowires attach through van der Waals interactions (Figure 1A,F). Typically, single pods or multipods are of wurtzite-phase arms grown on either a wurtzite or a zinc blende nucleus, respectively. HRTEM analyses show that a bipod nanowire consists of wurtzite arms epitaxially grown in the 001 direction on the {111} faces of a zinc blende core (Figure 1E).[7] The measured interplanar distances between the (111) faces of the zinc blende core and the (002) faces of the wurtzite arms are 3.20 and 3.16 Å, respectively, corresponding to known values.

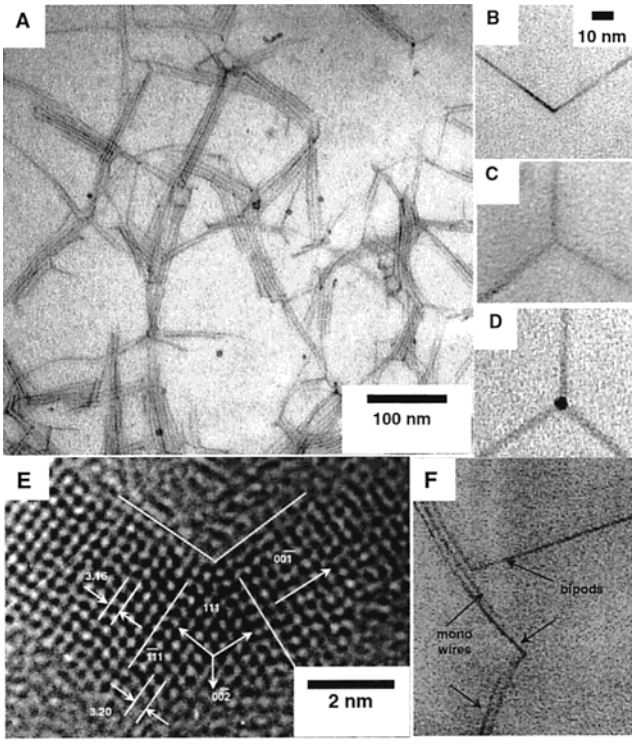

Figure 1. TEM images of MnS nanowires grown at 120 °C (A), a bipod (B), a tripod (C), a tetrapod (D), a HRTEM image of a bipod (E), and assemblies of mono- and bipods (F).

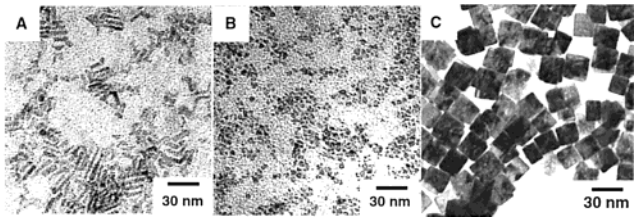

Figure 2. Shape evolution of MnS nanocrystals by the variation of growth temperatures: wires at 150 °C (A), spheres at 180 °C (B), and cubes at 250 °C (C).

Under similar growth conditions, varying either the growth temperature or the reaction time results in additional shape control of the MnS nanocrystals. As the growth temperature is increased to ~150 °C, monowire formation dominates with a 10-fold decrease in the aspect ratio (~8) to a size of 2.4 ± 0.3 nm in width (Figure 2A). As the growth temperature is increased further to ~180 °C, the exclusive formation of 0-D spheres with a diameter of 2.5 ± 0.3 nm is observed (Figure 2B). Finally, at much higher growth temperatures (~250 °C), only cube-structured MnS are obtained with a size of ~30 nm (Figure 2C).

Alternatively, growth time also plays an important role in shape control of the nanocrystals. Prolonged heating (~2 h) of the samples at 150 °C instead of 180 °C induce the same conversion of wires to spheres. Figure 3 shows shape evolution of MnS nanocrystals that arises from varying the growth time. After ~20 min from the precursor injection, monowires of 2.5 ± 0.3 nm is observed (Figure 3A). However, gradual deformation of the wires appears at ~1 h (Figure 3B), and complete sphere formation occurs after 2 h (Figure 3C).

(6) Kuno, M.; Lee, J. K.; Dabbousi, B. O.; Mikulec, F. V.; Bawendi, M. G. *J. Chem. Phys.* **1997**, *106*, 9869.
(7) Jun, Y.-W.; Lee, S.-M.; Kang, N.-J.; Cheon, J. *J. Am. Chem. Soc.* **2001**, *123*, 5150.

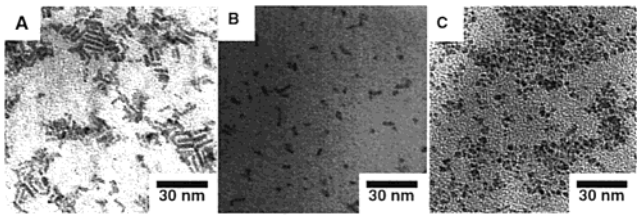

Figure 3. Time-dependent shape evolution of MnS grown at 150 °C: 20 min (A), 1 h (B), and 2 h (C). As the growth time increases, the shapes of MnS nanocrystals gradually change from rods to spheres.

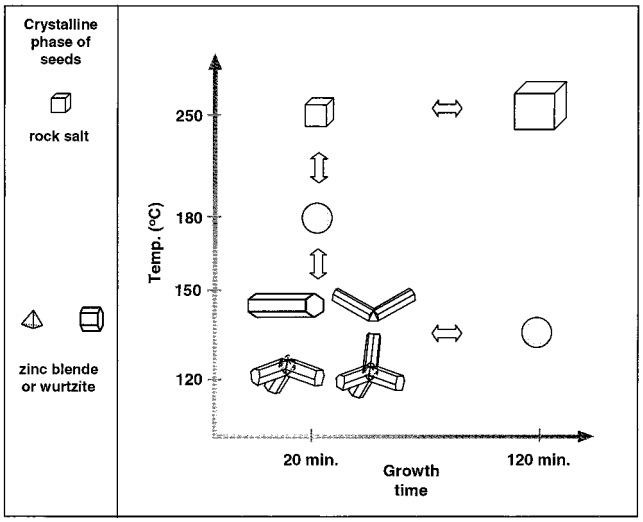

Figure 4. Shape change map of MnS nanocrystals.

There are at least two factors that are responsible for the shape determination of the MnS nanocrystals. The first is the crystallographic phases of the initial seeds. At lower temperatures (<200 °C), the initial formation of nuclei with either a zinc blende (β-MnS) or a wurtzite (γ-MnS) phase and subsequent crystal growth results in sphere or wire shapes.[2] On the other hand, at higher temperatures (>200 °C), the presence of nuclei of rock salt (α-MnS) phase induces the formation of cubes.[8] The second factor is the delicate balance between the kinetic and thermodynamic growth regimes. In the kinetic regime, fast growth on the crystallographic faces with high surface energy promotes 1-D formation. However, when sufficient thermal energy is supplied either by utilizing higher growth temperatures (~180 °C) or heating for extended periods of time (e.g., ~2 h at 150 °C), the more thermodynamically stable spherical shapes are favored through the intraparticle 1-D to 2-D ripening and interparticle Ostwald ripening processes.[2] The growth scheme of MnS nanostructures is summarized in Figure 4.

These new architectures exhibit unique spectroscopic features. UV−Vis absorption and photoluminescence spectra of the MnS wires of 2.2 nm in width (aspect ratio of ~80) and spheres (2.5 nm) show quantum-confined blue shifts of the absorption band edges from the bulk value of 3.2 eV (Figure 5). The observed absorption band edges occur at 3.64 and 3.53 eV while the photoluminescence band maxima occur at 3.34 and 3.46 eV for wires and spheres, respectively. In addition, a Stokes shift

(8) According to the literature, for MnS, two metastable phases (β and γ) are preferred at low temperatures, whereas a stable rock salt phase (α) is exclusive at higher temperatures (>200 °C). See (a) Macintyre, J. E. *Dictionary of Inorganic Compounds*, 1st ed.; London: New York, 1992. (b) Lu, J.; Qi, P.; Peng, Y.; Meng, Z.; Yang, Z.; Yu, W.; Qian, Y. *Chem. Mater.* **2001**, *13*, 2169.

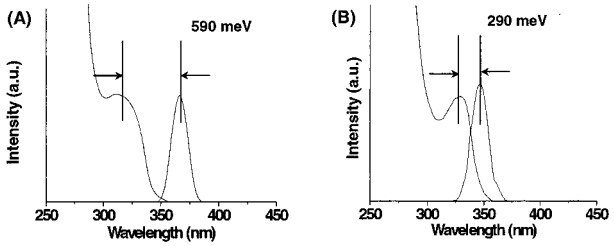

Figure 5. Absorption and photoluminescence spectra of MnS nanocrystals: wires (A) and spheres (B).

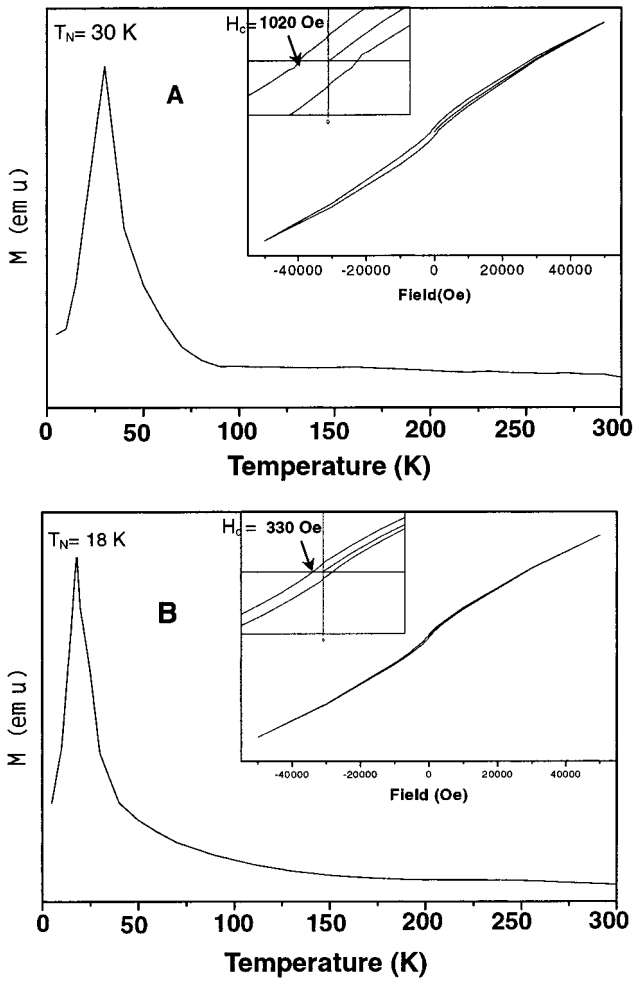

Figure 6. ZFC curves and hysteresis loops (inset) of MnS nanocrystals: 2.2 nm nanowires (A) and 2.5 nm nanospheres (B).

(590 meV) that is 2 times larger than that of the spheres (290 meV) is observed for the wires.[2] Our MnS nanowires show antiferromagnetic behavior with a Neel temperature (T_N) of 30 K shifted from the bulk value of 90 K with a coercivity (H_c) of 1020 Oe measured at 5 K. In comparison, spheres of similar size (~2.5 nm) show a decrease in both T_N (18 K) and H_c (330 Oe), possibly due to a loss of shape anisotropy (Figure 6).[2]

Until now, the studies on colloidal DMS nanocrystals have mainly been focused on 0-D dots.[9,10] We now present Mn-doped

(9) (a) Wang, Y.; Herron, N.; Moller, K.; Bein, T. *Solid State Commun.* **1991**, *77*, 33. (b) Bhargava, R. N.; Gallagher, D.; Hong, X. Nurmikko, A. *Phys. Rev. Lett.* **1994**, *72*, 416. (c) Feltin, N.; Levy, L.; Ingert, D.; Pileni, M. P. *J. Phys. Chem. B.* **1999**, *103*, 4.

(10) For example, Bawendi and co-workers[11a] reported observation of a large decrease (~4-fold) of doped Mn atoms even after first pyridine exchange experiment of $Cd_{1-x}Mn_xSe$ samples.

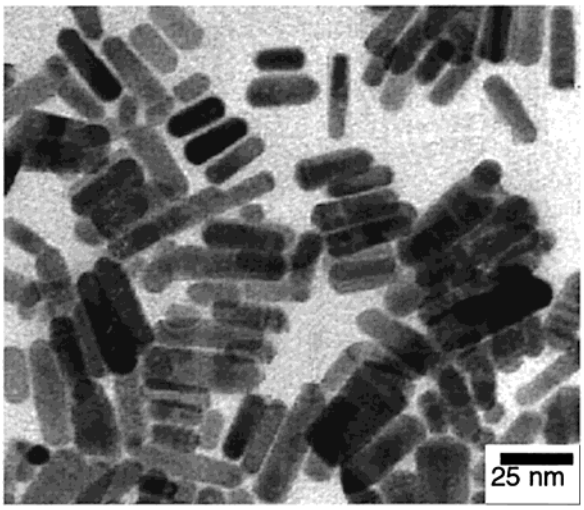

Figure 7. TEM image of $Cd_{0.88}Mn_{0.12}S$ wires of ~7 nm in width with aspect ratio of ~4.

1-D $Cd_{1-x}Mn_xS$ nanorods synthesized from appropriate amounts of the dopant precursor, $Mn(S_2CNEt_2)_2$, mixed with a CdS precursor, $Cd(S_2CNEt_2)_2$, at 120 °C. TEM and EDAX analyses show that the $Cd_{1-x}Mn_xS$ nanorods are ~7 nm in width with an aspect ratio of ~4 at maximum doping levels up to ~12% (Figure 7). Except in some cases,[9] the formation of DMS nanocrystals with a homogeneous distribution at high level of Mn doping has been difficult because of easy segregation of Mn dopants from the host matrix. Therefore, to confirm homogeneous distribution of Mn atoms inside the CdS matrix, ligand exchange experiments with pyridine were first performed, which removes Mn atoms bound to the surfaces of host nanocrystals. In the case of Mn atoms residing on the surfaces of host matrix, a huge decrease of Mn composition is expected.[10] However, in our study of $Cd_{1-x}Mn_xS$ rods, even after repeated (three times) ligand exchange processes, only slight decreases of Mn composition appeared in EDAX analyses of four different doping levels: from 1.88% to 1.61%, from 4.50% to 4.12%, from 9.18% to 8.48%, and from 13.43% to 12.45%. This result indicates Mn atoms are not heavily localized on the surfaces of nanocrystals.

Embedding of Mn inside the matrix is also inferred from EPR measurements. Because hyperfine splitting constants depend on the environments of Mn atoms, the bonding characteristics between Mn atoms and host lattices can be explained by EPR analysis. Figure 8 shows EPR spectra of ligand-exchanged $Cd_{1-x}Mn_xS$ nanorods with various compositions of Mn atoms. In the case of low concentrations of Mn (~2%), six hyperfine splittings due to Mn ($I = {}^5/_2$) were clearly observed along with a Lorentzian curve pattern that is attributed to Mn−Mn interactions (Figure 8A), and the observed splitting constant is 64.8×10^{-4} cm^{-1}. This value is consistent with the occupation of Mn on T_d sites of internal CdS matrix according to literature values.[12] In contrast, much larger hyperfine splittings of 83×10^{-4} cm^{-1} were reported, where the Mn atoms are mainly localized near the surface layers of the CdSe hosts.[11a] With increasing Mn concentration (~4% and ~8%), the overall

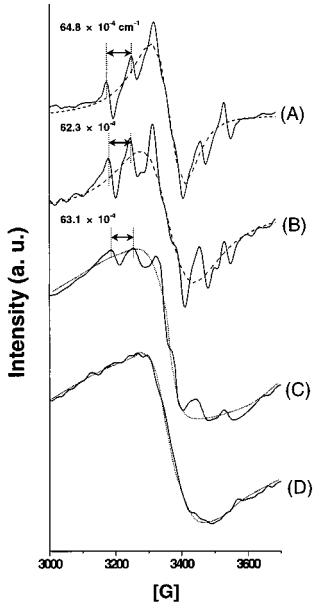

Figure 8. EPR measurements of $Cd_{1-x}Mn_xS$: $x = 0.02$ (A), 0.04 (B), 0.08 (C), and 0.12 (D).

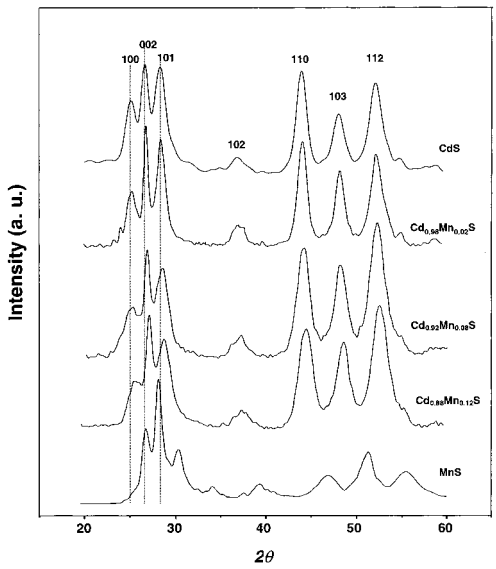

Figure 9. X-ray diffraction patterns of $Cd_{1-x}Mn_xS$. It is observed that the peaks are gradually shifted to higher angles as the Mn composition (x) increases.

Lorentzian shapes become gradually broader due to the increased the Mn−Mn interactions (Figure 8B,C). However, the hyperfine splitting constants remain almost identical with values of ~62.3 $\times 10^{-4}$ and 63.1×10^{-4} cm^{-1}, respectively. In the case of higher than 12% Mn, even though we cannot extract hyperfine splittings due to significant broadening of Lorentzian curves (Figure 8D), X-ray diffraction studies indicate some clues on the distributions of Mn atoms inside the matrix.

Further structural evidence is obtained by X-ray diffraction analyses. Our obtained $Cd_{1-x}Mn_xS$ nanorods show a gradual decrease in lattice constants as the Mn composition (x) is increased from 0 to 0.02, 0.08, 0.12, and 1 (Figure 9). Changes in the lattice constants from 4.093 to 4.083, 4.069, 4.059, and 3.873 Å for the a axis and from 6.696 to 6.675, 6.631, 6.616, and 6.376 Å for the c axis are observed with the increase in Mn composition (x) from 0 to 0.02, 0.08, 0.12, and 1. These

(11) (a) Mikulec, F. V.; Kuno, M.; Bennati, M.; Hall, D. A.; Griffin, R. G.; Bawendi, M. G. *J. Am. Chem. Soc.* **2000**, *122*, 2532. (b) Norris, D. J.; Yao, N.; Charnock, F. T.; Kennedy, T. A. *Nano Lett.* **2001**, *1*, 3.
(12) Kennedy, T. A.; Glasser, E. R.; Klein, P. B.; Bhargava, R. N. *Phys. Rev. B* **1995**, *52*, R14356.

trends are consistent with Vegard's law[13] and indicate homogeneous distribution of Mn inside the CdS matrix even with 12% Mn doping. In our attempt for incorporation of much higher amounts of Mn atoms (e.g., $>\sim$15%), however, segregation of Mn atoms out of the CdS matrix is observed.

On the basis of our studies and those of others,[4] mild growth conditions are needed for high-level doping of Mn. For example, at high temperature ($\sim$300 °C) with otherwise identical procedures, only poorly doped $Cd_{1-x}Mn_xS$ nanorods ($x < 0.02$) resulted in our study, where most of the Mn atoms seem to be annealed out of CdS lattices under supply of sufficient thermal energy.

In summary, a one-pot strategy for the shape- and dopant-controlled synthesis of nanocrystals has been successfully developed in a monosurfactant system. The factors involved in determining their shapes are elucidated in part: the crystalline phase of the initial nuclei and balanced control between kinetic and thermodynamic growth regimes are essential in determining the final architecture. Our studies demonstrate that, with the proper choice of precursors for both the matrix and the dopant, it is possible to prevent these problems through a low temperature (e.g., $\sim$120 °C) assisted kinetic growth process and the introduction of MnS monomer species that can be easily incorporated into the CdS matrix due to its compatible ionic bonding characteristics. Our synthetic method is straightforward, with potential for mass production, and also can be extended to the synthesis of other kinds of magnetic semiconductors with various architectures.

Acknowledgment. This work was supported by the KRF (Grant KRF-2000-015-DS0023).

JA016887W

(13) (a) Furdyna, J. K. *J. Appl. Phys.* **1998**, *64*, R29−R24. (b) Kim, K.-W.; Cowen, J. A.; Dhingra, S.; Kanatzidis, M. G. *Mater. Res. Soc. Symp. Proc.* **1992**, *272*, 27−33.